

Effect of the Coarsening of Austenite Grain on the Microstructure and Corrosion Behavior of a Cold Rolled AISI 316Ti Stainless Steel

Houria Kaddour^{1,*}, Fatah Hellal², Ahmed Haddad³, Zoheir Boutaghout³.

¹ Materials Sciences Laboratory, Faculty of Chemistry, USTHB, BP 32, 16111, El Alia, Bab Ezzouar, Algiers, Algeria

² Ecole Nationale Polytechnique, Département de Métallurgie, LSGM, BP 182, 16051, El Harrach, Algiers, Algeria

³ Research Center in Industrial Technologies CRTI, P.O. Box 64, Chéraga, Algeria

*E-mail: hkaddour@usthb.dz

Received: 2 April 2022 / Accepted: 10 May 2022 / Published: 6 June 2022

The effect of coarsening of austenite grain on microstructure and corrosion behavior of AISI316Ti austenitic stainless steel, during cold rolling, has been investigated. The AISI 316Ti austenitic stainless steel has been heated at 1100°C for 3 hours, resulting in an average austenite grain size growth of 5 times. The steel was then cold-rolled at 20, 37, 56, and 88% deformation degrees. The characterization of the microstructure has been assessed using optical microscopy, scanning electron microscopy, and X-ray diffractometry. Electrochemical properties have been evaluated by using a scanning Kelvin probe (SKP). Microstructural analysis showed that cold deformation without prior heating leads to the growing formation of strain-induced α' -martensite, as cold deformation increases. But, the microstructure obtained after subsequent cold rolling and preheat treatment was almost exempt from induced α' -martensite. The grain growth due to heat treatment, the effective titanium content of austenite, and the strain rate during cold rolling steps are factors that influence the strain-induced α' -martensite transformation. SKP, in air, demonstrated that the plastic deformation decreased the ability to passivation of the surface. The results obtained show that at high cold rolling, the heat treatment before the cold rolling can improve the electrochemical behavior of AISI 316Ti austenitic stainless steel.

Keywords: AISI 316Ti stainless steel, heat treatment, cold rolling, strain-induced martensite, SKP.

1. INTRODUCTION

It's well known that austenitic stainless steels are identified by γ -austenite phase stability. Their relative ease of manufacturing and their great resistance to uniform corrosion explain their application in a wide variety of fields. They are thus used in chemical, petrochemical, and pharmaceutical industries, in food and beverage equipment, as well as in the production of tanks for the transport of aggressive

substances. The structural stability of austenitic stainless steels in a large temperature range allows for their use at low temperatures for the storage of liquid gases, and high temperatures in heat exchangers. Austenitic stainless steels are however sensitive to grain growth upon heating, but due to their face-centered cubic lattice, they usually remain ductile and protected against embrittlement [1,2].

Austenitic stainless steels are unstable under mechanical stress. Indeed, cold working can induce the formation of strain-induced martensite, which can improve their mechanical properties but, unfortunately, can also decrease their good resistance to corrosion [3, 4]. Strain-induced martensite(or α' -martensite) depends on austenite stability (chemical composition and austenite grain size) and rolling conditions (strain amount, temperature, and rolling rate) [5]. Lo et al. [6], Hedayati et al. [5] and Meric de Bellefon et al. [7] pointed out that M_{d30} temperature (the deformation temperature at which 50% in volume of martensite is formed after a true tensile strain of 30%) and the stacking fault energy of the austenitic stainless steels are important factors which control the amount of induced martensite.

Amounts of titanium, higher than the standard values, are adopted during heat treatments and in thermo-mechanical processes to stabilize the austenite and delay the martensitic transformation [8]. Steigerwald [9] found that the theoretical value of titanium needed to stabilize the stainless steel can be calculated by the equation:

$$\% \mathbf{Ti}_{th} = 5(\% \mathbf{C} + \% \mathbf{N}) \quad (1)$$

The addition of titanium in austenitic stainless steel leads to the formation of carbides and nitrides that are much more stable than chromium carbides ($Cr_{23}C_6$). As mentioned in Padhila's review [10], these precipitates show two types of distribution:

(i) a coarse dispersion, 1–10 μm in size, of primary particles formed during solidification; and (ii) a fine dispersion, 5–500 nm in size, of secondary precipitates. In stabilized steels, some of the primary carbides can be dissolved during the solution heat treatment at temperatures ranging from 1050 to 1150°C, and then they precipitate in the shape of fine secondary precipitates during the aging heat treatment or when these materials are subjected to high-temperature applications.

The MC carbide precipitation is predominantly intragranular, on dislocations and stacking faults. However, MC precipitation at grain boundaries can also occur. This leads up to structural hardening and reduced susceptibility to intergranular corrosion [8, 11, 12] caused by chromium carbides.

Several works have been interested in the effect of grain size on the rate of α' -martensite induced by plastic deformation. V. Shrinivas and al. [13] reported that the amount of α' -martensite increases with decreasing grain size in AISI 304 stainless steel, while in AISI 316 stainless steel, the amount of α' -martensite is independent of grain size and, therefore, the chemical composition also plays an important role in the formation of α' -martensite.

In contrast, Varma and al. [14] have shown that in AISI 304 and 316 plates of steel, the deformation is accentuated by large grain size. Kisko and al. [15] found that large grain size promoted α' -martensite during cold rolling deformation of austenitic stainless steel 15Cr-9Mn-Ni-Cu. On a lesser scale, Jung and al. [16] mentioned that, in the case of metastable austenitic steel with ultrafine grain size, the decrease in the grain size leads to greater stability of the austenite and retards the production of α' -martensite.

On another side, under the mechanical solicitation, the passive film can be broken and the latticed defects (dislocations and slip bands) reach the surface in the shape of emerging steps, with variable

heights. These surface heterogeneities affect the electrochemical processes and particularly the adsorption of oxidizing species and the potential for dissolution [17, 18].

Specific electrochemical measurement techniques (scanning vibrating electrode technique and scanning Kelvin probe) and corresponding parameters are nowadays increasingly used [19, 20]. They are much consistent with a local behavior approach, with an interest in the elements of the microstructure (grains, boundaries, phases, precipitates, lattice defects...).

As there is little information available on the effect of the coarsening austenite grain due to high-temperature pretreatment and chemical content, in the case of cold-rolled AISI 316Ti austenitic stainless steels compared the 316/316L grades, the present work aims to highlight the effect of Ti and growing austenitic grain on the α' -martensite induced by strain after cold rolling, and on the evolution of defects lattice from bulk the surface, as well as the evolution of passive film.

2. EXPERIMENTAL PROCEDURE

A commercially available AISI 316Ti stainless steel has been investigated. Its chemical composition, as shown in Table 1, was determined by optical emission spectrometry.

Table 1. Chemical composition of the material used in this study.

Elements	C	Cr	Ni	Mo	Mn	Ti	Si	N	S	Fe
Content (wt%)	0.034	16.52	10.41	2.02	1.69	0.48	0.38	0.028	0.017	Bal

Two samples, 160mm x 10mm x 5mm in size, have been prepared for cold rolling. One was used at receiving state (RS), and the other was heated (HT) at 70°C/min to 1100°C, kept at this temperature for 3h, to increase the austenitic grain size, and then quenched in water (Fig. 1). The two samples were respectively cold rolled up to 20%, 56%, and 88% deformation degree.

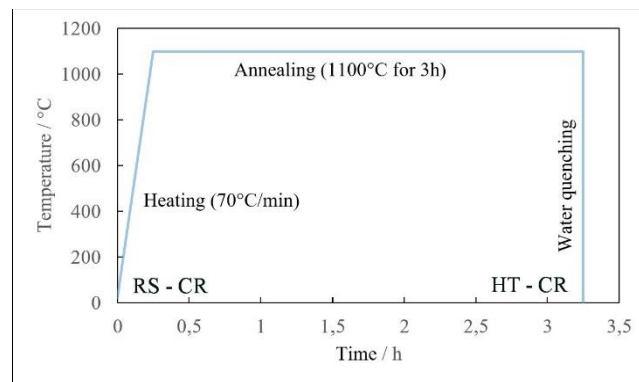


Figure 1. Schematic illustration of thermal treatment, with cold-rolled samples: received-state RS (left) and heat-treated HT (right).

For metallographic examinations, the samples were polished and then etched at 5 V in a 10% oxalic acid solution for 45s. The samples were examined under an optical microscope (Nikon Eclipse

LV100ND) and a scanning electron microscope (Zeiss Gemini SEM 300). The grain sizes were calculated using the linear intercept method and the mean intercept length.

The identification and evaluation of the transformation induced by the deformation of the samples were carried out by using an X-ray diffractometer (Bruker D8 Discover diffractometer with Co-K α source). X-ray diffraction (XRD) data were recorded in the 2 θ range from 30° to 120°. Phase analysis of XRD data was determined using the X'PertHighScoresoftware.

The scanning Kelvin probe (SKP), provided from the VersaSCAN platform, is used to characterize the surface material reactivity by measuring the Volta potential. The surface of specimens was prepared by grinding to 4000-grit, followed by final polishing using 3, 1, and 0.1 μm diamond paste. The sample was cleaned in an ultrasonic bath, degreased by ethanol, washed in deionized water, and dried in air. Measurements were carried out in the air, at ambient temperature. The SKP is calibrated using a standard Cu/CuSO₄ electrode, to establish a relation between the work function and Volta potential. The potential maps were analyzed by the mean of a needle, made with a flat-ended cylindrical Pt probe with a diameter of 250 μm . The probe vibrates perpendicularly to the surface with an amplitude of 20 μm and a frequency of 2 kHz. The sample-needle distance is defined manually before starting the scan.

The potential difference, or contact potential deviation, ΔV is defined as [21]:

$$\Delta V = \frac{\varphi_m - \varphi_{skp}}{e} \quad (2)$$

Where φ_m and φ_{skp} are the work functions of the metal and the probe material, and e is the electron charge. The Volta potential (φ/e) above the surface of the working electrode, measured by SKP, is proportional to the metal potential in the passive state [21,22].

3. RESULTS AND DISCUSSION

3.1. Microstructural characterization

Figure2a shows the AISI 316Ti microstructure of the RS sample. The austenitic grains are polygonal and uniformly distributed. They contain a high density of twins. After heat treatment, grain growth is observed (Fig. 2b). The average grain size achieved is about 90 μm , while it was about 15 μm at receiving state. It has been reported that grain growth in stabilized steels is only significant above 1050°C [23]. In addition, the two microstructures (Fig. 2a and 2b) show the presence of small regions of the δ ferritic phase and titanium carbide precipitates (TiC). The ferrite is located at the grain boundaries of the austenite, while the precipitates of titanium carbide are distributed within the austenitic matrix and at the grain boundaries.

The presence of δ -ferrite is characterized by EDS analyses (Fig. 3); their ratio is deduced from the Schaeffler diagram, in our case δ -ferriteratioisworth6%. It is well known that the amount of 2 - 6% ferrite in the microstructure has beneficial effects during the welding process.

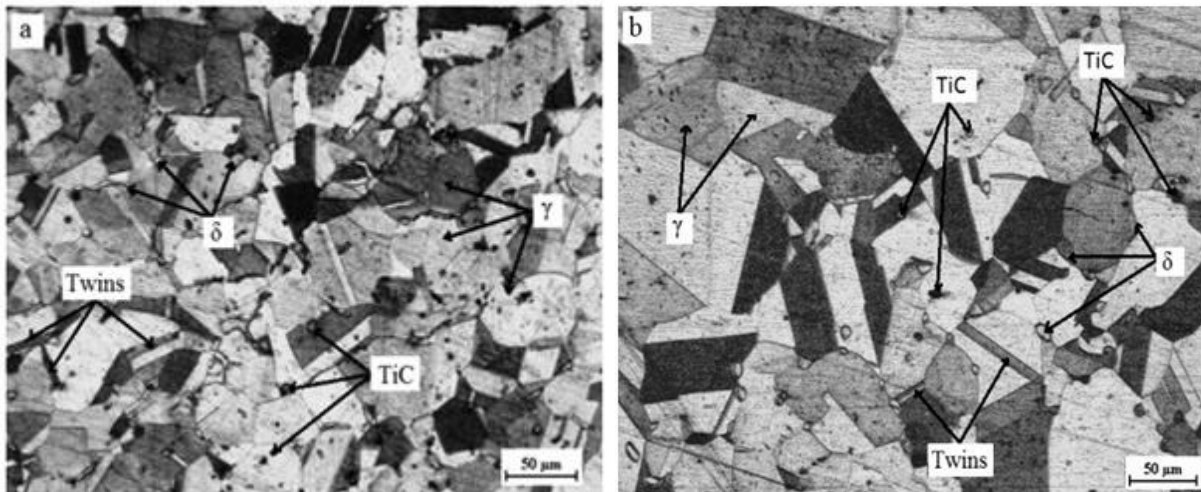


Figure 2. Microstructure of AISI 316Ti stainless steel, without cold rolling: (a) RS sample, (b) HT sample

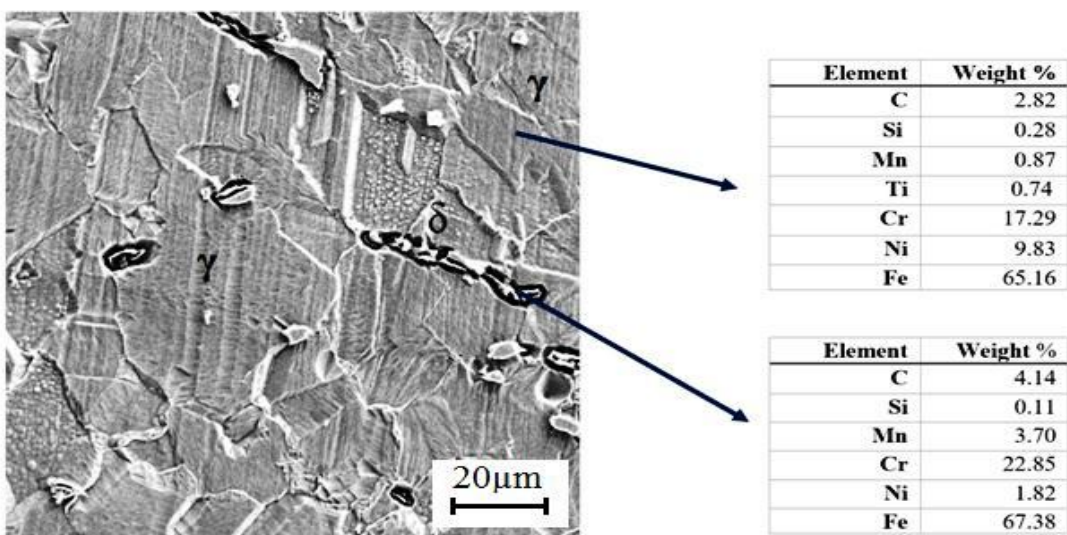


Figure 3. SEM micrograph and EDS characterization of AISI 316Ti stainless steel as-received

Titanium carbide precipitates are identified by their morphology, their bright contrast, and their average size which varies from $1\mu\text{m}$ to $15\mu\text{m}$ (Fig. 2a and 2b)[24-26].

As cold rolling is applied to AISI 316Ti, austenitic grains change at different scales. For RS samples with cold rolling from a 20% deformation degree, the formation of shear bands is observed (Fig. 3a). Talonen and al. [27] found that, at low strains, only narrow planar defects are visible and that, after exceeding a defined plastic strain, shear bands appear in austenitic grains, depending on the composition of the steel and the deformation temperature. After cold rolling at 37%, a certain amount of α' -martensite phase, dark-colored by etching, appears inside the austenite matrix. The presence of α' -martensite is further confirmed by XRD analysis (Fig.6). The presence of α' -martensite affects the uniformity of grains [28].

From 56% to 88% of cold rolling, emergences on the surface of shears bands appear inside austenitic grains and occur in the volume, leading to changes in the morphology of the surface (Fig. 4c and 4d).

At 88% of cold rolling, the grain boundaries become less detectable (Fig. 4d), so the equivalent grain size cannot be accurately calculated. On the other hand, the increase in plastic deformation induces a very finely dispersed α' -martensite and creates a pronounced relief inside the austenite grains [29].

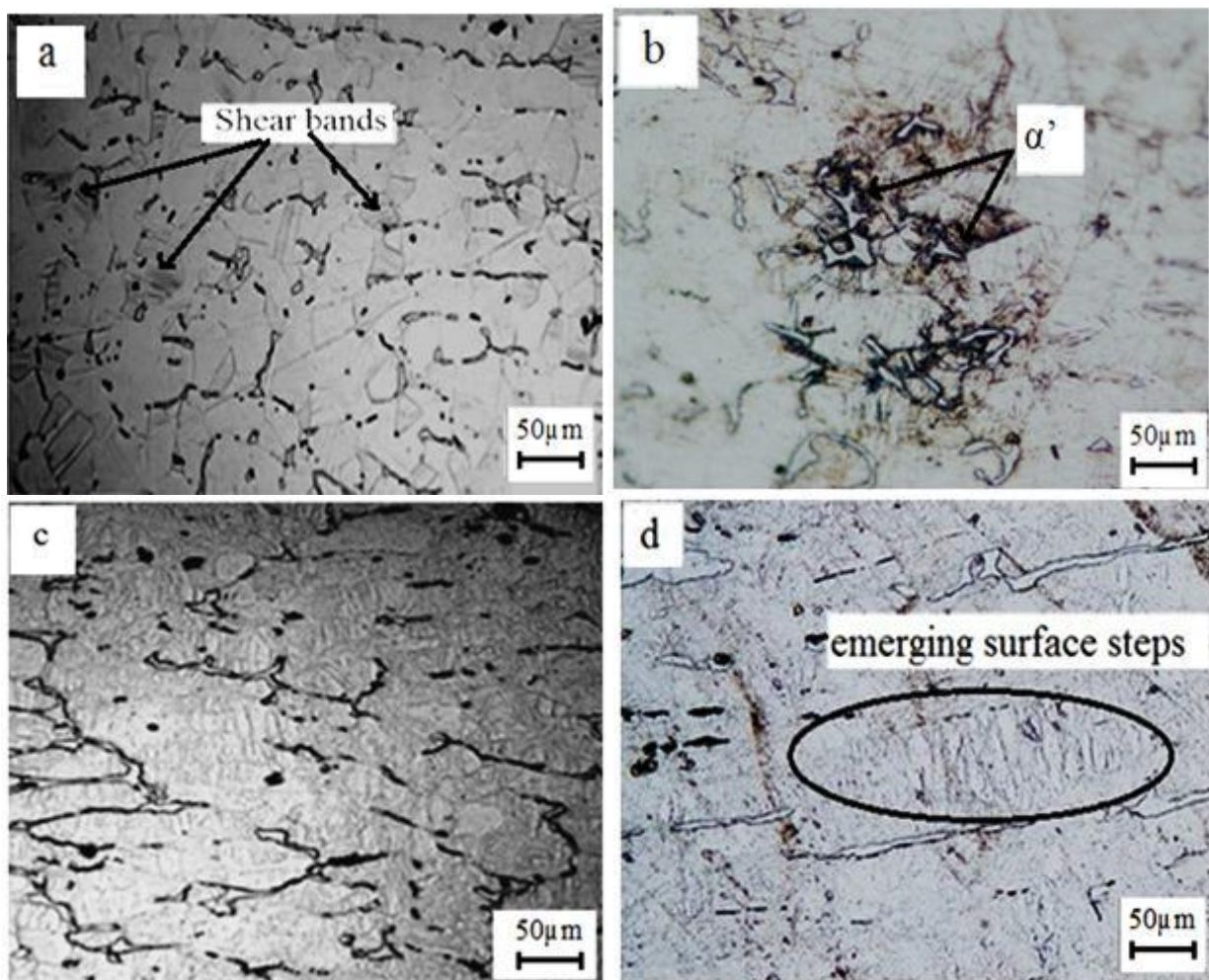


Figure 4. Microstructures of RS samples of AISI 316Ti after cold rolling: (a) 20%, (b) 37%, (c) 56% and (d) 88%.

Concerning the HT samples with cold-rolling, the microstructure of (Fig. 5a and 5b) indicates that, under low deformation degree, the density of the dislocations increases according to a non-uniform distribution within the austenite grains. But, as the rolling ratio increases, the densification of these defects allows them to reorganize and form primary dislocations pile-ups until they reach the surface of the sample in the shape of emergent steps (Fig. 5c and 5d).

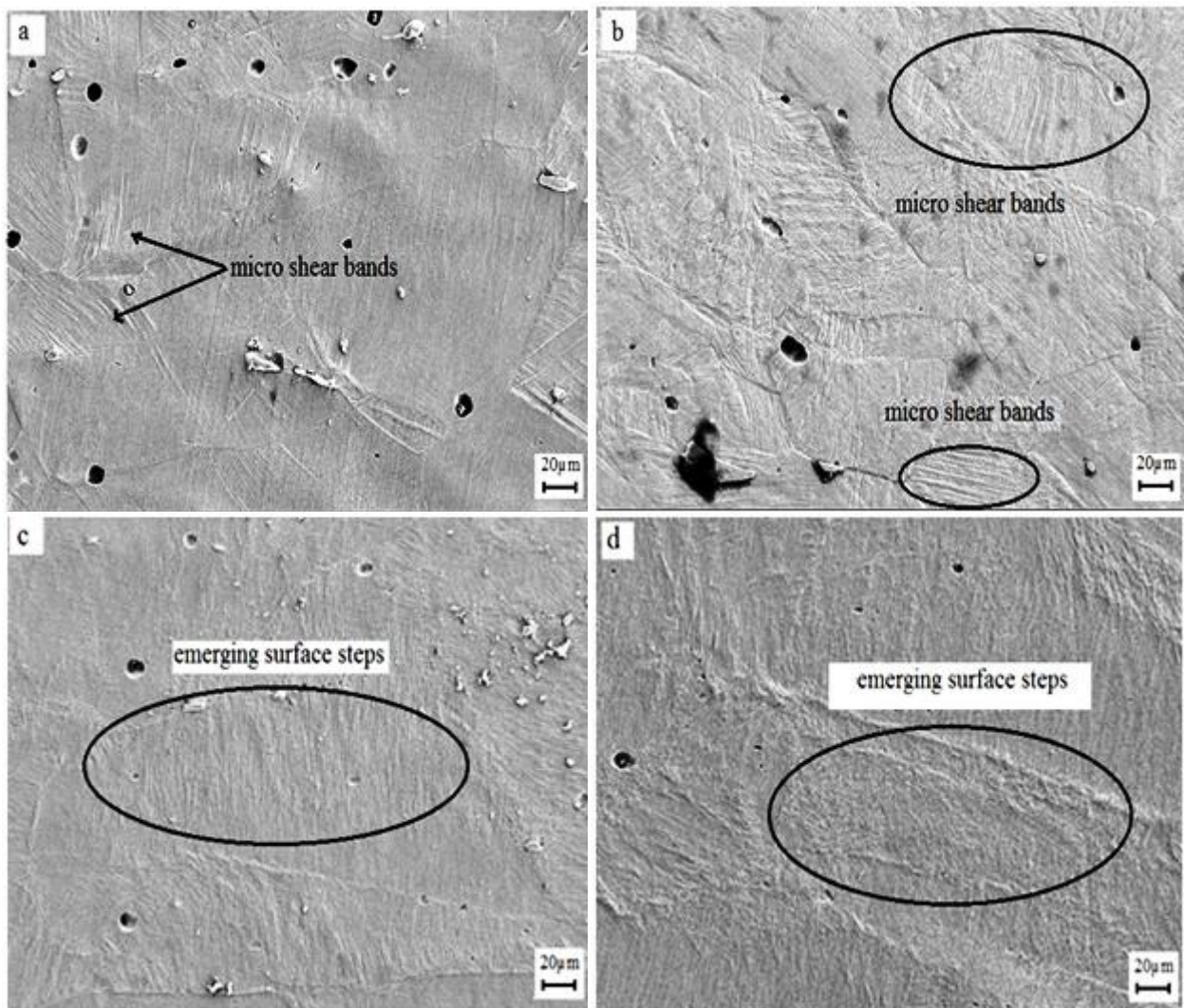


Figure 5. Microstructures of HT samples of AISI 316Ti after cold rolling: (a) 20%, (b) 37%, (c) 56% and (d) 88%.

X-ray diffraction analysis was performed in this study for the quantitative evaluation of α' -martensite in AISI 316Ti steel, and the comparison between RS and HT samples. The volume fraction of α' -martensite was calculated with the formula of Yang and Luo, 2000) [30]:

$$V_{\alpha'} = \frac{\left(\frac{1}{n}\right) \sum_{i=1}^j \left(\frac{I_{\alpha'}^j}{R_{\alpha'}^j}\right)}{\left(\frac{1}{n}\right) \sum_{i=1}^j \frac{I_{\gamma}^j}{R_{\gamma}^j} + \left(\frac{1}{n}\right) \sum_{i=1}^j \frac{I_{\alpha'}^j}{R_{\alpha'}^j}} \quad (3)$$

where n is the number of each of the present phases, I is the integrated intensity of the peaks, and R is the material scattering factor. The values of R used in this work are given in Table 2 [30, 31]. The change in the volume fraction of α' -martensite with cold rolling is shown in (Fig.6b).

Table 2. X-ray reflections and R_i values, in the quantitative determination of the volume fraction of α' -martensite.

Reflection	$d(\text{Å}^\circ)$	Angle diffraction $2\theta (\circ)$	R_i
$\gamma(111)$	2.070	51.21	212
$\gamma(200)$	1.793	59.87	95
$\gamma(220)$	1.267	89.78	52
$\alpha'(110)$	2.026	52.38	279
$\alpha'(200)$	1.433	77.24	40

At 37% of cold rolling, XRD spectrums highlight the presence of α' -martensite. Considering the following expression to estimate stacking fault energy (SFE) from chemical composition [7]:

$$\text{SFE}(\text{mJ.m}^{-2}) = 2.2 + 1.9\text{Ni} - 2.9\text{Si} + 0.77\text{Mo} + 0.5\text{Mn} + 40\text{C} - 0.016\text{Cr} - 3.6\text{N} \quad (4)$$

The evaluation for AISI 316Ti equals 24mJ.m^{-2} . This value allows us to conclude that α' -martensite is formed directly from austenite ($\gamma \rightarrow \alpha'$) and not first by the formation of ϵ martensite ($\gamma \rightarrow \epsilon \rightarrow \alpha'$). This observation agrees well with Kaoumi and al. [32], who showed that materials with low stacking fault energy ($<18\text{mJ.m}^{-2}$) follow an indirect transformation sequence, while materials with high stacking energy ($>18\text{mJ.m}^{-2}$) prefer the direct transformation sequence.

As shown in (Fig.6a and 6b), the proportion of α' - martensite increases with cold rolling up to 37%, due to the intensification of formation of dislocations within austenite grain [33] and, consequently, the densification of shear bands. It has been reported [13, 34] that the number of non-parallel shear bands increases with strain and that some of the shear band intersections become the nucleation site for α' -martensite.

From 37% to 56% of cold rolling, a small quantity of α' -martensite is formed, due to a slight mechanical disorder [35], inducing a decrease in the movement of the dislocations. As a result, the dislocation sublattice reorganizes in dense areas, next to pre-existing shear bands [36, 37]. This result can be also explained by the effect of adiabatic heating [38]. In fact, throughout the multi-pass cold rolling, the strain rate increases and gives a certain rise in temperature. Since SFE depends on temperature, nucleation of α' - martensite will be inhibited.

At 88% cold rolling, the diffraction peak (110) of α' -martensite becomes more intense than the peak (111) of austenite (Fig. 6a). When the strain ratio is very high, a new surface is created between the austenite and α' -martensite during the distortion of the austenitic matrix, replacing the usual boundary at the austenite-martensite interphase [39].

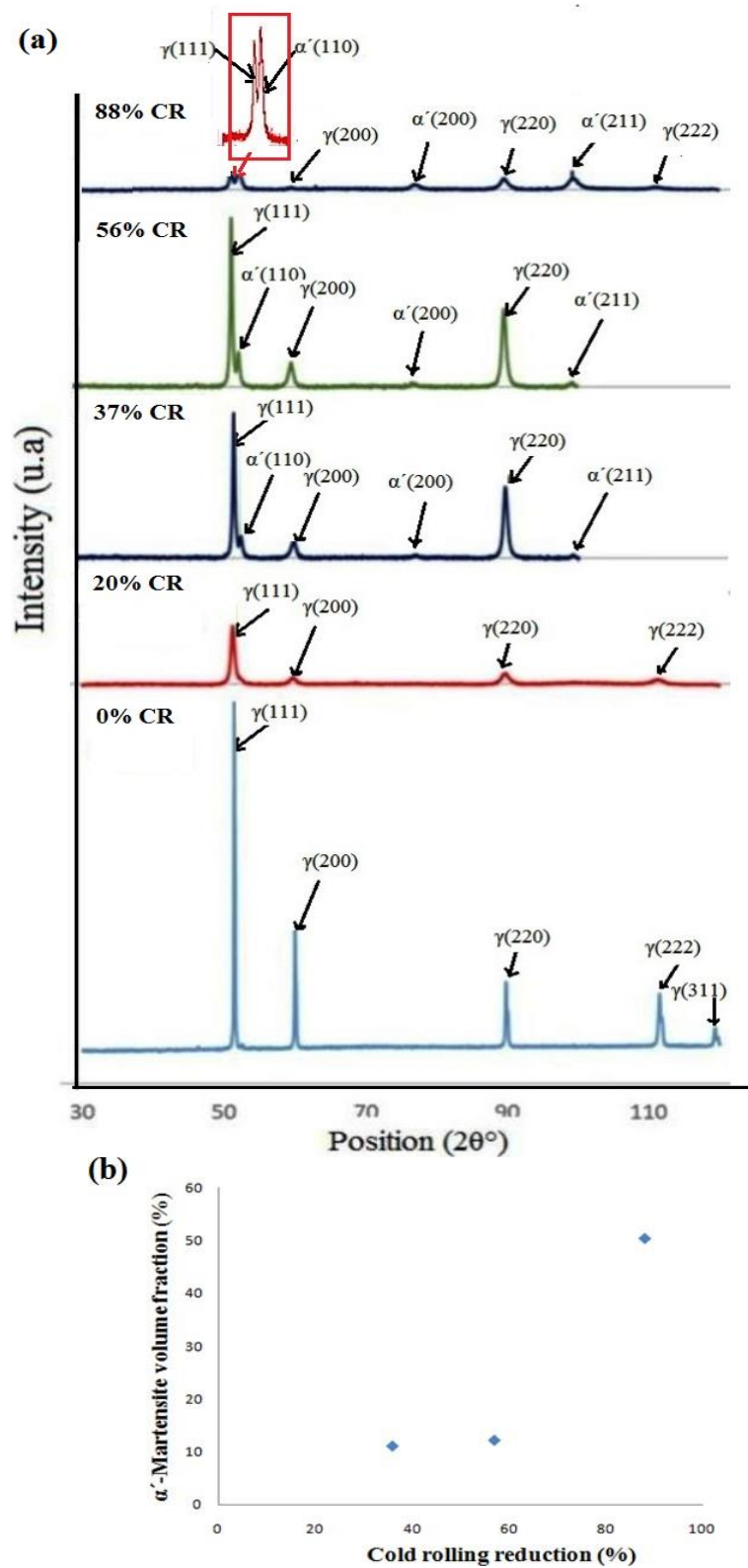


Figure 6. (a) XRD analysis of AISI 316Ti stainless steel for RS samples, as a function of deformation degree, and (b) calculated volume fraction of α' -martensite of RS sample.

Regarding the HT samples with cold rolling, no presence of α' -martensite remains detectable in the XRD diagram (Fig.7). The explanation may lie in the size of the austenite grains. The grain enlargement, resulting from the long heating to 1100°C, can prevent the reorganization of dislocations, from scattered networks to cells, and thus delays the formation of secondary pile-ups. It has been shown, in tensile tests [15], a continuous increase in dislocation density within grains, as well as near grain boundaries, as strain increases. This densification is further accelerated inside the grains, at high values of tensile strain.

Under the effect of cold rolling, the growth of the grain size of austenite induces a decrease in the energy at the grain boundaries, compared to the grains. Indeed, if the elastic deformation energy is consumed by the creation of the defects, the plastic deformation energy remains stored inside the hardened metal. As a result, the number of intersection sites of the shear bands will be considerably reduced, which will limit the nucleation sites of α' -martensite. The density, movement of dislocations, and their interaction are profoundly affected by grain volume.

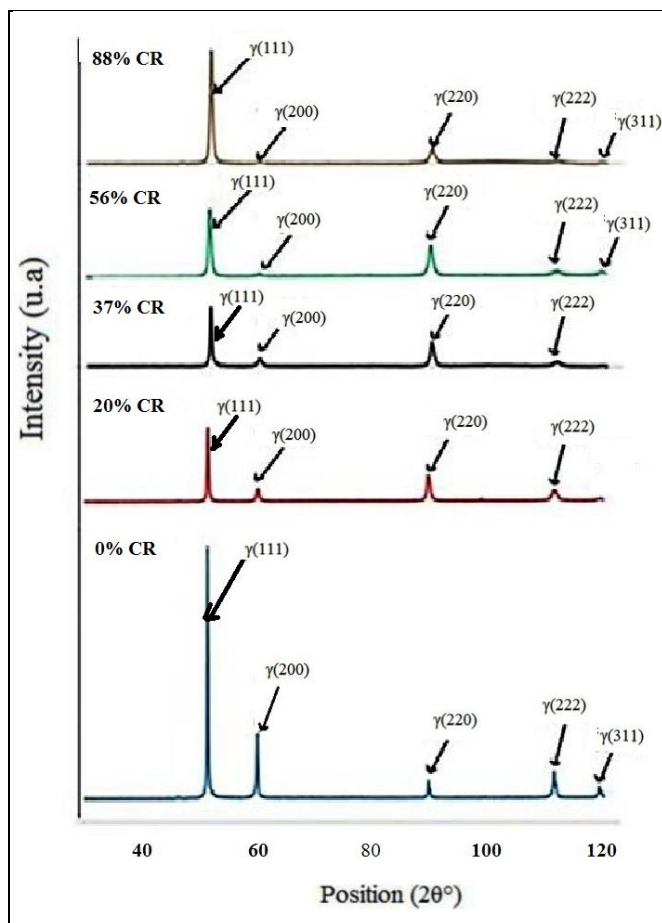


Figure 7. XRD analysis of AISI 316Ti stainless steel for HT samples, as a function of deformation degree.

On the other hand, the widening of the peaks, observed in the two stainless microstructures, is due to the formation of plastic micro-deformations induced by the stresses. In addition, the changes in

the intensity of the different peaks are due to the transformation of the γ -austenite phase to α' -martensite and the change in texture caused by cold rolling [40].

The microstructure after heat treatment is much more homogeneous than in the reception state (Fig. 2a and 2b). This is due to the movement of grain boundaries and the dissolution of certain carbides. Large carbides partially dissolve, while small ones dissolve completely, increasing the carbon content of the solid solution. The SFE increases and gives more stability to the treated microstructure.

In addition, titanium should improve martensitic transformation because, under stress conditions, it decreases the stability of the austenite phase by reducing its SFE [38]. The presence of TiC carbides results in carbon depletion in the austenite, an increase in the temperature of M_{d30} , and a decrease in SFE. This implies lower stability of the austenite and, therefore, an increase in the sensitivity to the formation of α' -martensite in RS samples.

On the other hand, it has been reported that due to the twinning phenomenon, small grains are less stable than large grains. Mechanical twinning is more pronounced in large grains and leads to inhibition of α' -martensite formation [40].

The effect of the cold rolling ratio and the coarsening austenite grain due to high-temperature pretreatment has been studied by the SKP technique. Volta potential maps (Fig.8) show that the potential values measured by SKP depend on several parameters. The main parameters are the chemical composition of phases, α' -martensite, crystallographic defects (dislocations and slip bands), donor-acceptors density, passive film thickness, emerging surface steps, and surface roughness [8, 18, 41]. The effect of increasing plastic strain on Volta potential is presented in Table 3.

Table 3. Volta potential of AISI 316Ti.

Conditions	Cold rolling (%)	Volta potential (mV)
As-received state	20	1490–1710
	56	53–187
Heat-treated	0	804–1040
	20	273–437
	56	79–228

In the case of an as-received state with a 20% of deformation degree, Volta potential varied in the range 1490-1710mV. This potential decreased in the range 53-187mV for a 56% ratio. The same behavior was observed after heat pretreatment. Volta potential evolved in the ranges 273-437mV and 79-228mV, respectively for 20% and 56% ratios.

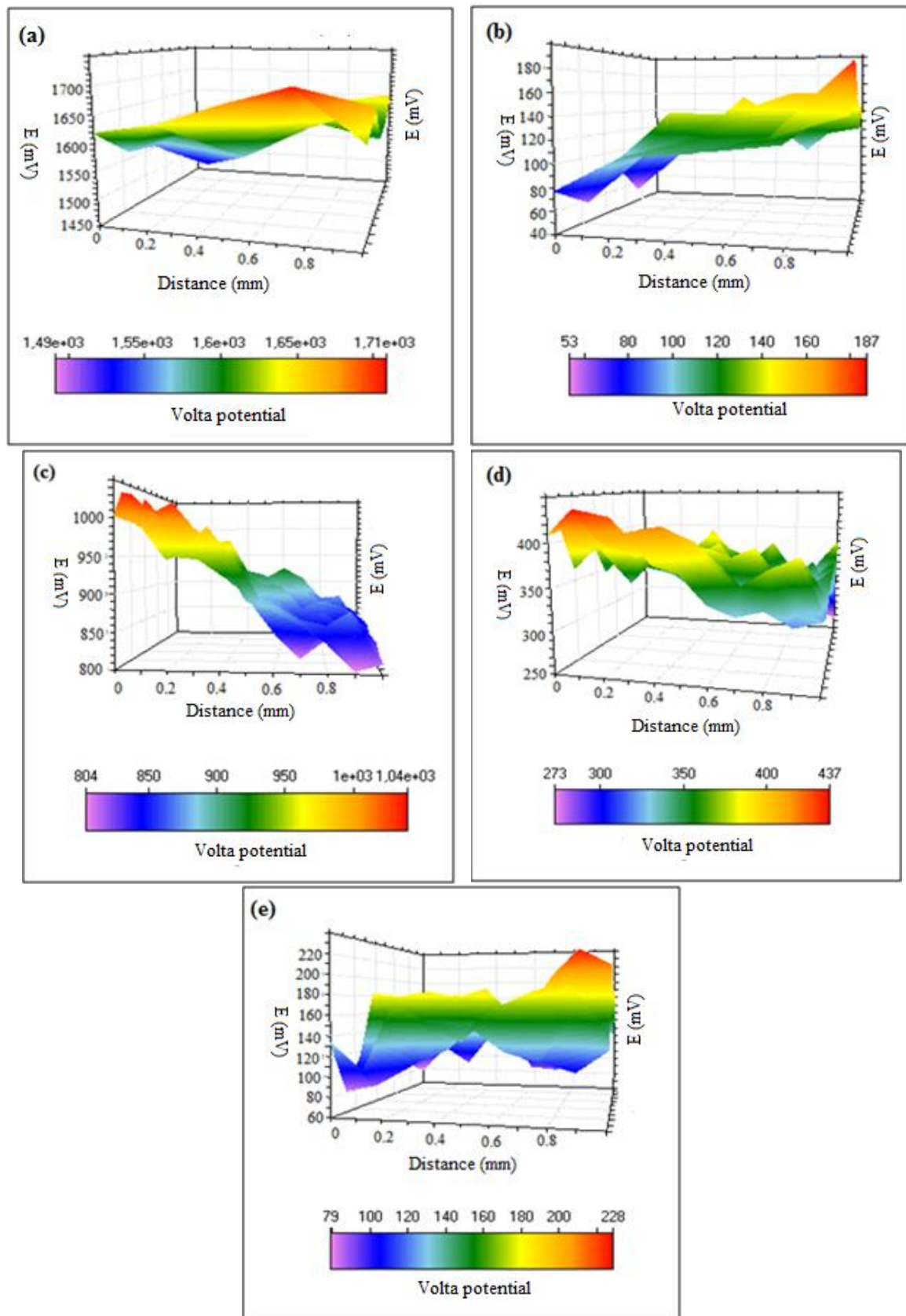


Figure 8. Volta potential maps of AISI 316Ti, (a) as-received states with cold deformation of 20%, (b) as-received state with cold deformation of 56%, (c) undeformed after heat treating, (d) after heat treatment with cold deformation of 20% and (e) after heat treatment with cold deformation of 56%.

The decrease in the potential, explained by the formation of new surfaces, is related to high electrical activity and a great electronic conductivity of the oxide passive film. The plastic strain induces pile-ups, which emerge on the surface and increase its roughness. Thus they give rise to thinning of the oxide passive film [28, 42]. This film loses its homogeneity and then its protective feature [43].

From one part, it's known that the creation of dislocations causes local fluctuation at the Fermi-level electron. This makes the Fermi-level electrons, close to the dislocations, binds less strongly to the surface so that it is easy for them to escape, lowering thus the potential [22]. From another part, the evolution of the passive film leads to the creation of a dipole between oxygen molecule (negative charge) and oxide film (positive charge) consequence, the conductivity and the capacitance of the oxide film increase and the potential decreases. Moreover, the presence of the induced α' -martensite phase can also influence the oxide film activity [41].

The second part of the analysis concerns the evolution of Volta potential, under the effect of prior heat treatment of AISI 316Ti stainless steel. At a low cold rolling ratio, i.e. 20%, the preheating reduces the potential, which can be related to the effect of the larger grain size. As reported in the literature, the reduction of grain size leads to the formation of a more compact and uniform passive film [44, 45]. But for a higher cold rolling ratio, i.e. above 56%, the potential becomes higher, which can be related to the effect of the absence of α' -martensite. As α' -martensite is found in deformed areas, the passivation ability of the stainless steel decreases. Heat pretreatment can then be considered, at high deformation, as a favorable factor for electrochemical behavior.

4. CONCLUSIONS

This study focused, in the case of an austenitic stainless steel 316Ti, on the effect of preheat treatment and the influence of the effective titanium content on the microstructure, strain-induced α' -martensite transformation, and corrosion behavior. A grain size, five times greater than that of the reception state sample was obtained by heat treatment at 1100°C for 3 hours. The main results of the study are presented below:

- Due to the cold rolling of the as-received stainless steel, the stress caused the nucleation of a sublattice of dislocations and shear bands. These led to the transformation of a part of the γ -austenite phase into α' -martensite, induced by strain. The more the deformation degree, the greater the quantity of α' - martensite.
- When stainless steel is heated for 3 hours at 1100°C, then cold-rolled, the absence of α' -martensite is observed. The enlargement of the austenite grain allows a greater consumption of the elastic strain energy. This prevents the reorganization of dislocations from the dispersed network into a cellular network. As a result, the number of intersection sites of the shear bands will be greatly reduced, which may limit the number of α' -martensite nucleation sites.
- Small-grained austenite is less stable than coarse-grained austenite, due to the influence of the twinning. The mechanical twinning is more pronounced in coarse grains, which inhibits the formation of α' - martensite.
- The addition of titanium decreases the stability of the austenite phase and improves α' -

martensite transformation. Therefore, the precipitation of TiC can, by reducing the amount of C in solid solution, influence the formation of α' -martensite.

The electrochemical results, obtained by using the local technique SKP, show that in the case of heat pretreatment with 56% of cold rolling, the Volta potential becomes higher than that of the as-received state, which can be related to the effect of the absence of α' -martensite. As α' -martensite is found in deformed areas, the passivation ability of the stainless steel decreases. Therefore, preheating can then be considered, at a high deformation ratio, as a favorable factor for electrochemical behavior.

CONFLICTS OF INTEREST

The authors declare that they have no conflict of interest.

References

1. M. F. McGuire, *ASM International*, MP, Ohio, (2008) 70.
2. P.M.O. Silva, H.F.G. Abreu, V.H. Albuquerque, P.L. Neto and J.M.R.S. Tavares, *Mater. Des.*, 32(2011) 605.
3. G. Monrrabal, A. Bautista, S. Guzman, C. Gutierrez and F. Velasco, *J. Mater. Res. Technol.*, 8(2018)1335.
4. N. Srinivasan, S.S. Kumaran and D. Venkateswarlu, *Mater. Res. Express.*, 6(2018) 1.
5. A. Hedayati, A. Najafizadeh, A. Kermanpur and F. Forouzan, *J. Mater. Process. Technol.*, 210(2010)1017.
6. K.H. Lo, C.H. Shek and J.K.L. Lai, *Mater. Sci. Eng.*, 65(2009) 39.
7. G. Meric de Bellefon, J.C. Van Duysen and K. Sridharan, *J. Nuclei. Mater.*, 492(2017) 227.
8. A.Z. Farahat and T.A. El-Bitar, *Mater. Sci. Eng. A*, 527(2010) 3662.
9. R. Steigerwald, Metals Handbook, Vol. 13, Metals Park (OH): *ASM International*, (1990) 123.
10. A.F. Padilha and P.R. Rios, *ISIJ Int.*, 42(2002) 325.
11. S. Xu, X.Q. Wu, E.H. Han, W. Ke and Y. Katada, *Mater. Sci. Eng. A.*, 490(2008) 16.
12. A. Pardo, M.C. Merino, A.E. Coy, F. Viejo, M. Carboneras and R. Arrabal, *Acta Mater.*, 55(2007) 2239.
13. V. Shrinivas, S.K. Varma and L. E. Murr, *Metall. Mater. Trans. A*, 26(1995) 661.
14. S.K. Varma, J. Kalyanam, L.E. Murr and V. Shrinivas, *J. Mater. Sci. Lett.*, 13(1994) 107.
15. A. Kisko, R.D.K. Misra, J. Talonen and L.P. Karjalainen, *Mater. Sci. Eng. A*, 578(2013) 408.
16. Y.S. Jung, Y.K. Lee, D.K. Matlock and M.C. Mataya, *Met. Mater. Int.*, 17(2011) 553.
17. A. Nazarov, V. Vivier, D. Thierry, F. Vucko and B. Tribollet, *J.Electrochem. Soc.*, 164(2017) C66.
18. A. Barbucci, G. Cerisola and P.L. Cabot, *J. Electrochem. Soc.*, 149(2002) B534.
19. C.H. Paik, H.S. White and R.C. Alkire, *J. Electrochem. Soc.*, 147(2000) 4120.
20. H. Krawiec, V. Vignal, E. Finot, O. Heintz, R. Oltra and J.M. Olive, *Metall. Mater. Trans. A.*, 35(2004) 351.
21. A. Nazarov and D. Thierry, *Electrochem. Acta*, 52(2007) 7689.
22. N.F. Casals, A. Nazarov, F. Vucko, R. Pettersson and D. Thierry, *J.Electrochem.Soc.*, 162(2015) C465.
23. A.F. Padilha, R.L. Plaut and P.R. Rios, *ISIJ Int.*, 43(2003) 135.
24. W. Kesternich and D. Meertens, *Acta Metall.*, 34(1986) 1071.
25. Å. Gustafson, *Mater. Sci. Eng. A*, 287(2000) 52.
26. B. Zhao, W. Zhao, H. Shi, G. Li and Y. Ding, *Eng. Fail. Anal.*, 105(2019) 961.
27. J. Talonen and H. Hanninen, *Acta Mater.*, 55(2007) 6108.
28. H. Luo, H. Su, G. Ying, C. Dong and X. Li, *Appl. Surf. Sci.*, 425(2017) 628.

29. J. Liu, C. Chen, Q. Feng, X. Fang, H. Wang, F. Liu, J. Lu and D. Raabe, *Mater. Sci. Eng. A.*, 703(2017) 236.
30. J. Wang and L. F. Zhang, *Anti-Corros. Method M.*, 64(2017) 252.
31. V. Tandon, A.P Patil and R.C. Rathod, *Mater. Res. Express.*, 5(2018) 1.
32. D. Kaoumi and J. Liu, *Mater. Sci. Eng. A*, 715(2018) 73.
33. T. Shintani and Y. Murata, *Acta Mater.*, 59(2011) 4314.
34. H. Jun-Xia, Y. Xiao-Ning and X. Zhou, *J. Iron Steel Res. Int.*, 19(2012) 59.
35. D. Treppmann and E. Hornbogen, *J. Phys. IV*, 07(1997) 211.
36. U. F. Kocks and H. Mecking, *Prog. Mater. Sci.*, 48(2003) 171.
37. A. Borbely and J.H. Driver, *Mater. Sci. Eng. A*, 387(2004) 231.
38. A. Dasa, S. Tarafder and P. C. Chakraborti, *Mater. Sci. Eng. A*, 529 (2011) 9.
39. D.M. Xu, X.L. Wan, J.X. Yu, G. Xu and G.Q. Li, *Metals*, 8 (2018) 1.
40. M.M. Wang, C.C. Tasan, D. Ponge, A. Kostka and D. Raabe, *Acta Mater.*, 79(2014) 268.
41. A. Nazarov, V. Vivier, F. Vucko and D. Thierry, *J. Electrochem.Soc.*, (2019) 3207.
42. N. Jadhav and, V.J. Gelling, *J. Electrochem. Soc.*, 166(2019) C3461.
43. G. Grundmeier, K. Jüttner and M. Stratmann, *A Comprehensive Treatment*, Wiley. (2013) 285.
44. M.J.K. Lodhi, K.M. Deen and W. Haider, *Materialia*, 2(2018) 1.
45. K. BinTayyab, A. Farooq,A. Ahmed Ali, A. Basit Nadeem and K.M. Deen, *Int. J.Miner.Metall. Mater.*, 28(2021) 440.